Phase diagram and equation of state of praseodymium at high pressures and temperatures

Bruce J. Baer, Hyunchae Cynn, Valentin Iota, and Choong-Shik Yoo
Lawrence Livermore National Laboratory, University of California, Livermore, California 94550

Guoyin Shen
GSECARS, Advanced Photon Source, Argonne National Laboratory, Argonne, Illinois 60439
(Received 28 May 2002; revised manuscript received 16 January 2003; published 30 April 2003)

The phase diagram for praseodymium (Pr) has been determined for pressures between 5 and 60 GPa and temperatures between 295 and 830 K using both *in situ* energy- and angle-dispersive x-ray diffraction with externally heated diamond-anvil cells. Mineral oil and argon were alternatively used as pressure media in order to compare conflicting results in the literature and to ensure the validity of mineral oil as an inert medium. Evidence for the presence of an, as yet, unidentified phase (denoted Pr-VI) above 675 K has been observed, whereas no compelling evidence has been observed for the existence of the recently reported monoclinic phase (Pr-V). The new constraints of the phase diagram, therefore, suggest that the phase transitions occur as Pr-I(dhcp)→Pr-II(fcc)→Pr-VI→Pr-IV(α-U) above approximately 700 K. Additionally, there is a Pr-III(distorted fcc), Pr-VI, and Pr-IV triple point at approximately 675 K and 23.8 GPa. Temperature-dependent equations of state have been determined, allowing the temperature-dependent volume collapse at the transition between Pr-III and Pr-IV to be calculated. We report a linear decrease of the volume collapse along the Pr-III to Pr-IV boundary with temperature, $\Delta V/V\ (\%) = 16.235 - 0.0156[T(\mathrm{K})]$; the extrapolation indicates that the volume collapse should vanish well below the melting point. With the temperature-dependent equation of state data and new phase diagram we demonstrate that the volume collapse can be accounted for by a change in the multiplicity of Pr atoms as the *f* electrons go from localized to itinerant.

DOI: 10.1103/PhysRevB.67.134115 PACS number(s): 64.30.+t, 61.50.Ks, 81.30.Bx

INTRODUCTION

Crystal structures and phase diagrams of valence-band *f*-electron transition metals, lanthanides and actinides alike, are important for understanding the effects of *f*-electron correlation and bonding.[1,2] The large volume-collapse transition in praseodymium (Pr), for example, is a good example of the electronically induced structural change from a high-symmetry closed-packed (or near closed-packed) fcc (or distorted fcc) structure to a relatively low-symmetry orthorhombic α-uranium (α-U) structure. The stability of high-symmetry low-pressure phases has been understood in terms of localized *f* electrons, as in many cases of rare-earth and *d* electron transition metals.[3] The low-symmetry high-pressure phases, on the other hand, have been understood in terms of itinerant *f* electrons, which participate in bonding and become more susceptible to low-symmetry distortions in crystal structure. This is the case for light actinides.[2,4]

An analogous volume-collapse transition, due to the delocalization of *f* electrons, occurs in cerium (Ce) at 0.7 GPa and 300 K, from γ(fcc)-Ce to α(fcc)-Ce with a 16% volume change at 0.7 GPa and 300 K.[5,6] This isostructural transition, however, is terminated at a critical point, 550 K and 1.8 GPa, and at higher temperatures the γ(fcc) phase directly transforms to low-symmetry α' (monoclinic or α-U)-Ce and upon further compression to ε(tetragonal)-Ce. The *f* electrons are considered to be well delocalized in both α'- and ε-Ce.[6] All the postulated γ/α, α/α', α'/ε phase boundaries roughly extrapolate to the same point, the unusual melting minimum near 950 K and 3 GPa.[7,8]

Although Ce and Pr are two of the most distinctive elements reporting large volume collapses from 10% to 16%, other lanthanides such as Pm and especially Gd also have phase transitions with notable volume changes at high pressures.[1,9,10] The delocalization of *f* electrons also commonly occurs in many light actinides (thorium to plutonium) at high pressures as well as across the whole actinide series at ambient pressure.[2] Because of its general importance, there have been an extensive amount of theoretical and experimental studies addressing various aspects of the volume-collapse transition in the literature.[1–11] However, it is important to note that the previous studies concentrated extensively on Ce and were largely restricted to ambient temperature. Furthermore, no single theory has successfully described the two governing phases of the volume-collapse transition simultaneously.[1] Therefore, the goal of this study is to investigate the volume-collapse transition of Pr *in situ* at high temperatures and pressures. This data could better assist in the systematic understanding of volume-collapse transitions in *f*-electron systems.

The phase diagram of Pr exhibits profound polymorphism at high pressures and temperatures, which is in many regards analogous to that of Ce.[8] At ambient temperature, Pr undergoes a series of phase transitions from Pr-I(dhcp)→Pr-II(fcc)→Pr-III(distorted fcc, $R\bar{3}m$)→Pr-IV(α-U, $Cmcm$).[12] The Pr-IV phase, which appears above 20 GPa at 300 K, is then stable to at least 103 GPa.[13] A recent study, however, has reported an additional phase Pr-V(monoclinic, $C2/m$) at ambient temperature at pressures between Pr-III at 10 GPa and Pr-IV at 20 GPa.[13] Subsequently, the same report lowers the range for the distorted-fcc phase (Pr-III) to between 7 and 10 GPa. The transition between III (or V) and IV occurs with a large volume collapse 10% (or 14%); while no significant

volume changes were apparent between other transitions of the phases I, II, III, and V.[12,13]

At high temperatures, the melting curve and phase boundaries among the bcc phase, Pr-I, and Pr-II were established at relatively low pressures (below 8 GPa) based on an earlier differential thermal analysis study.[14] However, the melting curve has recently been extended to 60 GPa using laser heating.[15] The phase boundaries of Pr-II, Pr-III, and Pr-IV had been previously determined to 550 K and 22 GPa based on energy-dispersive x-ray diffraction (EDXD).[12] However, it is unfortunate that neither the unit-cell parameters (and thus equations of state) of the phases nor the temperature dependence of the volume-collapse transition was determined in that EDXD study. Nevertheless, those early studies extrapolated the phase boundaries and diagram of Pr to 30 GPa and 1400 K and indicated the triple point of Pr-III, Pr-II, and Pr-IV to be at approximately 537 K and 21 GPa.[12] It is important to note that with the exception of a single data point calculated from the shock Hugoniot curve, the phase diagram above 23 GPa and 550 K in temperature and above 1200 K and 8 GPa in pressure was constructed entirely based on the extrapolations of lower-temperature data using simple thermodynamic constraints.[23] Furthermore, the presence of a recently reported Pr-V phase in the phase diagram is unknown above room temperature. It is also important to note here that the earlier study[12] used mineral oil as a hydrostatic pressure medium, whereas the latter study[13] used no pressure-mediating fluid at all. Therefore, in this study we have carefully reinvestigated the phase diagram of Pr by using *in situ* synchrotron x-ray diffraction at high pressures and temperatures using either argon or mineral oil for the pressure medium.

The main results reported in this paper include (1) the phase diagram of Pr to pressures as high as 60 GPa and temperatures as high as 830 K, (2) the evidence of a new high-temperature Pr phase (denoted as Pr-VI), (3) the equation of state of Pr at ambient and elevated temperatures, (4) the temperature dependence of the volume-collapse transition, and (5) the calculation of the entropy change across the III-IV boundary using the Clausius-Clapeyron equation and its comparison to the entropy change due to a reorganization of *f* electrons from localized to itinerant.

EXPERIMENTS

For high-temperature experiments using mineral oil as the pressure medium, diamond anvil cells (DAC's) were heated to 700 K by an external heater (HBZ nozzle heater from Omega) wrapped around the cylinder part of our DAC's. This DAC could be further heated to 1200 K by using an internal microheater that surrounded the two diamond anvils and interposing gasket. The internal microheater was constructed in three parts: (i) a Pt heating wire wrapped around a small corundum torus, (ii) an insulating corundum block outside the Pt heater, and (iii) a four-hole plug. These four holes are used for holding two electrical leads, a thermocouple wire pair (*K*-type, Omega) and a small pipe for a purging gas (1% H_2 in Ar) intake. The temperature was measured at two places: the first is in contact with the diamond anvil and gasket, which is the place closest to the sample, and the second is at the table of the cylinder's diamond anvil. While these two measurements differ by as much as 10 K per 200-K temperature increase, in this paper we only report the temperature at the point closest to the sample.

Samples using an argon pressure medium were heated in a vacuum oven using a different type of microheater. This microheater was made with a coiled nichrome wire placed inside a hollow Al_2O_3 toroid. Alternatively, some of these samples were heated externally using a cable heater.

For some samples, praseodymium metal was kept under mineral oil before, during, and after loading into the DAC's to prevent contamination due to chemical reaction with air. Great care was taken to ensure that any fresh metal surface cut from the main specimen (a 10-g ingot of Pr with a 99.9% purity from Alfa Aesar) was prevented from being directly exposed to air. This was done once we observed that Pr metal foil quickly formed a light yellow green patina when there was no mineral oil to protect it. Mineral oil was chosen because it was reported to be chemically inert with Pr.[12] Any sample we analyzed that was loaded without mineral oil was not only contaminated by oxide formation but was not hydrostatic at high pressures (i.e., above 20 GPa) either. This could be observed by a broad ruby luminescence spectrum for those samples in which ruby was added as an independent check of pressure. For the samples loaded under an argon pressure medium, the praseodymium sample was cleaned of any oil and a fresh (shiny) surface was cut. The entire operation was done in a glovebox under an argon atmosphere with the sample void space being subsequently filled by liquid argon. In most samples, gold powder was added as the pressure sensor. The equation of state (EOS) of gold is well known[16] and has been computed for high temperatures and pressures. This makes the gold sensor more reliable than ruby at high pressures and temperatures.

For some experiments, we utilized angle-dispersive x-ray diffraction (ADXD) by using a focused monochromatic x-ray beam (20.0 keV) from beamline 10-2 at the Stanford Synchrotron Radiation Laboratory (SSRL). Image plate detectors were used to record the diffracted x rays from several *hkl* lattice planes up to $2\theta=40°$. Using a 30-μm x-ray collimator (Rikagu), it typically takes about 15 min to collect an ADXD pattern of Pr with a reasonably good signal-to-noise ratio. Because of the relatively long exposure time required of ADXD and the possibility of the reactivity of Pr with mineral oil at high temperatures, we used EDXD at the Advanced Photon Source (APS) for most high-temperature x-ray experiments. Typically, a good diffraction pattern could be obtained in less than 1 min. Almost all EDXD patterns were taken with the detector at $2\theta=10°$ (i.e., $Ed=71.18$ keV Å). Some EDXD measurements were also taken at the National Synchrotron Light Source (NSLS) and would require nearly 10 min of collection time. Overall, several hundred diffraction patterns, encompassing a wide range of temperatures and pressures, were obtained for the present study. All the samples were initially polycrystalline at ambient conditions. However, we often found that whenever a sample underwent a phase transition at high temperature, it had a tendency to anneal along several preferred orientations.

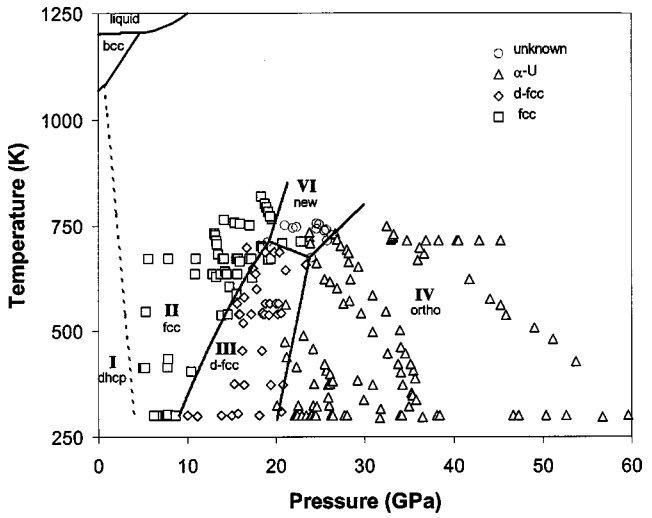

FIG. 1. Phase diagram of praseodymium. Open squares are the fcc phase, open diamonds the distorted-fcc phase, open triangles the α-U phase, and open circles are a new, as-yet, unidentified phase. The dhcp to fcc boundary is estimated from other results (see text) and is shown as a dashed line. All the boundaries above 1000 K are from Refs. 12, 14, and 15.

As a result, many of the diffraction patterns at high temperatures suffer from unusual peak intensities, which hampers characterization of the crystal structure of the new Pr phase reported in this paper. Further investigation of this structure is underway. Because of the added time required and the complexity associated with high-temperature experiments, no attempt was made to rotate the cell when obtaining a diffraction pattern, which would correct for any anomalies in peak intensity.

RESULTS AND DISCUSSION

The crystal structures of Pr determined to 60 GPa and 830 K in the present experiments are summarized in the phase diagram of Fig. 1. The ambient-pressure results of both the present and previous investigations[12,13] were used to help determine the pressure of each of the phase transitions at 300 K. Due to the sluggish nature of some of the phase transitions, we often observed hystereses, especially between the Pr-II and Pr-III phases. Phases II and III are very nearly identical since the distortion is less than 2% of the ideal packing for fcc. However, impurities, especially hydrogen, may also have an effect in shifting transition pressures and temperatures. It is possible that praseodymium's interaction with a mineral oil medium can generate hydrogen that is absorbed into the metal's lattice. Given the rapid pace that the EDXD patterns are taken, very little annealing time was allowed between successive data collections. Although our phase diagram shows a lack of points near the Pr-III (distorted fcc) and Pr-IV(α-U) phase boundary, this is not due to a lack of experimental data. Rather, it is due to the difficulty of consistently fitting the pattern with the known distorted-fcc (or trying to fit with the suggested monoclinic structure) or orthorhombic structure. Many of the patterns near this boundary could be fitted with those of previously identified Pr crystal structures, but have lattice parameters that contradict the larger body of data. Nevertheless, we do not suggest that these ''discarded'' data are useless, but that they require a much more complex analysis in which impurity, grain size, and nonhydrostatic effects can be taken into account.

Except for the newly identified phase, all the x-ray data were fitted based on previously published indexing.[17,18] We also assume that the atom positions of each phase do not change with pressure or temperature. This may have contributed to some of the difficulties in fitting, especially for the peak intensities. As mentioned above, the phase assignment and indexing were done in a manner as consistent as possible, yet this did not always yield a clear result. The c/a ratio indexed for the distorted-fcc phase at 13.8 GPa and ambient temperature was previously found to be 2.49,[17] only slightly greater than the $\sqrt{6}$ ratio for an ideal close-packed lattice of this type. Although it has also been reported that at 13.8 GPa the sample should be monoclinic,[13] we saw no evidence for this. All the distorted-fcc data we report in this study have a c/a ratio between 2.46 and 2.52 (about 1% from the previously reported value). We observed many patterns that could be indexed with an excellent fit to this crystal structure, but with c/a ratios that were outside this range. Since this phase has a diffraction pattern that is very close to a fcc pattern, and many peaks are identical in both, great care has been taken to ensure that these phases are distinguished properly. However, the volume difference is only about 1% and an indexing error here would not significantly affect the EOS, just the location of the phase boundary. It is possible that when the c/a ratio was outside the narrow range we assigned for it, internal strain, stacking faults, and/or unidentified phases could have caused the discrepancy.

The general appearance of our phase diagram is qualitatively in agreement with that of the previous study by Zhao, Porsch, and Holzapfel.[12] It is remarkable that, given the lack of diffraction peaks in that previous study, sufficient features could be distinguished to allow accurate phase assignment. However, their assignment of the superlattice $(\frac{5}{2}, \frac{3}{2}, \frac{1}{2})$ peak using the fcc basis is most likely the (223) or (217) reflection indexed to the distorted-fcc phase from Ref. 17. We also often observed that same peak diminish in intensity with increasing temperature, but other features of the phase remain. Since this is the only means used in the previous study[12] to distinguish Pr-II(fcc) from Pr-III(distorted fcc), it would explain why their Pr-II to Pr-III boundary has a shallower slope than that in our phase diagram. Another important difference in this work is that our phase diagram does not show a fcc to α-U phase boundary; this is due to the presence of a newly discovered high-temperature phase of Pr-VI above 675 K. The x-ray evidence of Pr-VI has been illustrated in Fig. 2. The low-pressure (below 8 GPa) high-temperature phase boundaries have already been explored.[14] That study shows the relationship between the dhcp, fcc, bcc, and liquid above 1000 K. The melting curve has been extended[15] to 60 GPa using laser heating and a triple point has been projected at about 24 GPa and 1400 K based on these earlier reports. Based on our phase diagram, that triple point would be for Pr-II, Pr-VI, and liquid at a slightly higher pressure.

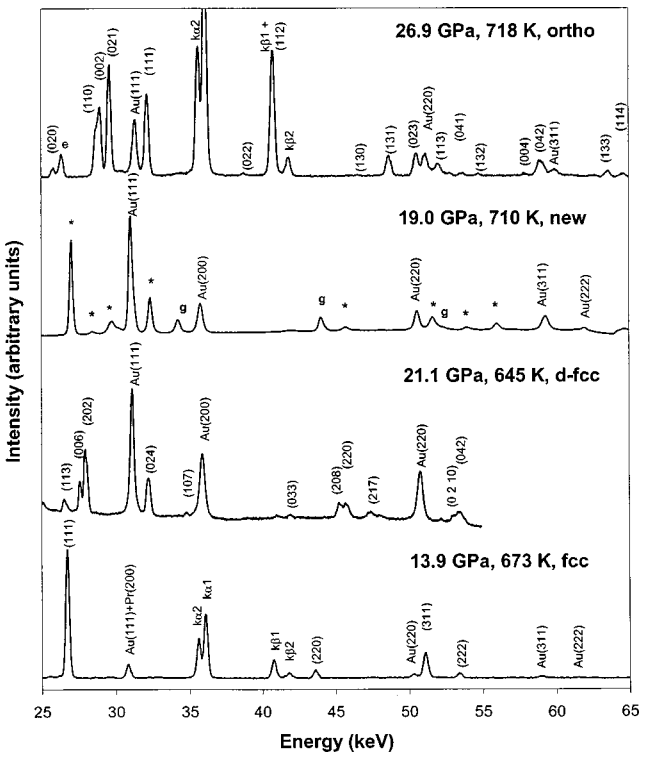

FIG. 2. Typical diffraction patterns for the various phases. (a) The fcc phase at 13.9 GPa at 673 K ($Fm\bar{3}m$, $Z=4$, $a=4.6131$), (b) distorted-fcc phase at 21.1 GPa and 645 K ($R\bar{3}m$, $Z=24$, $a=6.2157$, $c=15.4568$), (c) a new phase at 19 GPa and 710 K, and (d) orthorhombic phase at 26.9 GPa and 718 K ($Cmcm$, $Z=4$, $a=2.7330$, $b=5.4665$, $c=4.8769$). The *h* prefix is for the hydride phase, *e* for an escape peak, and *g* stands for gasket. The asterisks are the unindexed peaks of the new phase. The new phase and distorted-fcc patterns are converted from ADXD to match the energies of the other diffraction patterns taken by EDXD.

Figure 2 illustrates the typical differences in the diffraction patterns of Pr, as the pressure increases at high temperatures (680 ± 40 K). For a narrow region of temperature, the phase transitions in Pr occur as Pr-II(fcc)→Pr-III(distorted fcc)→new Pr-VI→Pr-IV(α-U). Above this region, phase III is no longer observed. Also, the diffraction patterns at 14, 21, and 27 GPa are very well described in terms of the crystal structures of three known phases, Pr-II(fcc), Pr-III(distorted fcc), and Pr-IV(α-U), respectively. The resulting lattice parameters are consistent with those identified at ambient temperatures. For example, the reported ambient-temperature structural parameters for Pr-III(space group $R\bar{3}m$, $Z=24$) at 13.8 GPa (Ref. 17) are $a=6.4699$ Å and $c=16.102$ Å and for Pr-IV(space group $Cmcm$, $Z=4$) at 23.3 GPa (Ref. 19) are $a=2.769$ Å, $b=5.619$ Å, and $c=4.851$ Å. The fcc superlattice reflection $(\frac{5}{2},\frac{3}{2},\frac{1}{2})$ of the previous study is not present in this distorted-fcc pattern. However, it is still consistent with the previous result,[12] showing a rapid decrease of the superlattice peak with increasing temperatures; for example, this peak is hardly detectable at 403 K in the earlier study.

We also report in Fig. 1 that the new Pr-VI phase exists up to at least 741 K and 25.7 GPa. Several diffraction lines (marked with a^*) are identified for this phase in Fig. 2; none of these lines correspond to those of the other known phases. This new Pr-VI phase appears reversibly from both Pr-III and Pr-IV above approximately 670 K. The determination of the crystal structure for this phase is very important. If it is another distorted-fcc phase, then there might be no volume collapse at the transition from Pr-II.

Additionally, none of the patterns in Fig. 2 could be indexed using the recently suggested Pr-V(monoclinic, $C2/m$) phase.[13] However, this does not rule out the possibility that there may be other polytypes present near the currently drawn Pr-III(distorted fcc) and Pr-IV(α-U) boundary. Every time we attempted to index a pattern from a sample within the distorted-fcc *P*, *T* regime as monoclinic, the result was a significant increase in specific volume with no improvement in the quality of the fit. Fitting with the suggested monoclinic structure[13] markedly inflates the volume collapse and, more importantly, makes the proposed distorted-fcc to monoclinic transition yield an increase in volume, which is unphysical. The presence of hydrogen in our samples is also an unknown factor. We do not know how much is present (due to being packed in mineral oil before use) and what effect it has on the transitions. However, we do not believe that this has significantly altered the phase boundaries. Comparisons with the samples loaded under argon result in a difference of, at most, 1 GPa and 40 K, the approximate size of our error bars for elevated temperature experiments. Impurities, grain size, and plastic deformation have been known to have a significant effect on the transition between the β(dhcp) and γ(fcc) phases of cerium.[11] Furthermore, sample preparation seems to have been the cause of many conflicting results in the relationship between the $C2/m$ and α-U phases of cerium.[11]

The presence of nonhydrostatic strains could distort the fcc or distorted-fcc lattice into a polytype. In such a case, the difference observed between the present and previous[13] results may be due to a lack of a hydrostatic pressure medium in the previous study. The assumption that Pr is a "soft" metal and does not require any hydrostatic medium does not necessarily hold up at high pressures, although the potential reactivity of Pr under extreme conditions clearly requires a carefully made selection of a pressure medium.

There is evidence that the selection of mineral oil is not entirely ideal; this is illustrated in Fig. 3. It demonstrates that Pr-IV(α-U) at 618 K and 26 GPa transforms to new Pr-VI (the peaks are marked with an asterisk) as the temperature is increased to 715 K. The reaction product, which initially coexists with the pure Pr phase, is shown as a series of new diffraction lines marked as $h(hkl)$ in the figure. Note that as the temperature is maintained at 723 K and 20 GPa, those new lines are enhanced, while the diffraction intensities from Pr-VI are diminished. Those new diffraction lines can be fitted very well to a fcc structure with the lattice parameter $a=4.7491$ Å at 723 K and 20.3 GPa. The lack of data points presented above 830 K in Fig. 1 is solely due to the fact that only this fcc pattern remains shortly after such high temperatures are reached and is irreversible. As the pressure is decreased, the *d* spacing of the fcc pattern approaches that of PrH_{2+x} $(0\leqslant x<1)$ under ambient conditions. [For PrH_2, $a=5.4856$ Å (Refs. 20 and 21).] Therefore, we conclude that

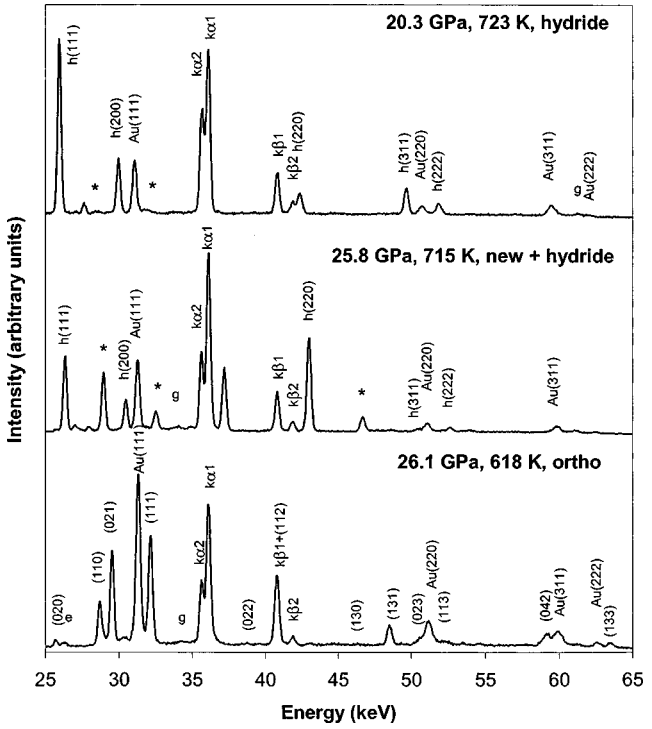

FIG. 3. The production of a hydride compound due to heating at high pressure. Lower panel: a typical orthorhombic pattern taken at 26.1 GPa and 618 K. Middle panel: Further heating (to 715 K) has transformed the orthorhombic phase to a new, as-yet unidentified, phase and has produced some hydride compound. Upper panel: The sample pressure has dropped a bit, but the transformation to hydride is essentially complete.

a chemical reaction occurs between Pr and mineral oil at high temperatures and pressures and forms a hydride. Once PrH_{2+x} is formed, the diffraction patterns indicating the presence of pure Pr-IV only reappeared when the pressure was markedly increased. However, the pure Pr-IV pattern disappeared again (with the hydride pattern reappearing) upon lowering the pressure at high temperature. It is not surprising that no such reaction has been observed in the previous experiments below 550 K at about 20 GPa. We also do not know if there is any catalytic activity for Pr under high pressure. No such reaction was observed when argon was chosen as the pressure medium, but the same phase relationships were observed. A more detailed study of the hydride will be published in the future.

Based on the large number of Pr diffraction patterns obtained in the present study, we were able to determine several isotherms of Pr at elevated temperatures as plotted in Fig. 4. Although we do not have diffraction patterns that clearly show the coexistence of the Pr-III(distorted fcc) and Pr-IV(α-U) phases at the transition, we are able to extrapolate from the many data points close to the pressures and temperatures that compose the transition line. The triple point for Pr-III, Pr-IV, and Pr-VI is extremely useful as an end point for this boundary. We have chosen five temperatures, including ambient, to calculate EOS's for the Pr-III(fcc) plus Pr-III(distorted fcc) phases and the Pr-IV(α-U) phase. Because of their similar crystal structures and compression behaviors, the two lower-pressure phases are treated together in this EOS fit. By using these data and presuming a linear temperature dependence of the three variables in the Birch-Murnaghan equation,[22] we are able to assign a small first-order temperature dependence of the bulk modulus at ambient pressure and high temperature $B_{0,T}$, its pressure derivative B', and specific volume $V_{0,T}$ at ambient pressure and high temperature. The data for 300, 540, 660, and 725 K have been graphed in Fig. 4. The data plotted in each of those graphs are within 40 K of the temperature listed for that graph, which is acceptable considering the small thermal expansion of Pr (about 0.1% in volume over 100 K). Each graph yields two EOS equations, one for the combined Pr-II and Pr-III phases and another for the Pr-IV phase. The B_0, V_0, and B' at 300 K were chosen to best fit both our data as well as those in the literature. The resulting parameters are summarized in Table I, together with their temperature dependence. It is important to remember that when extrapolating bulk modulus and volume to zero pressure for the Pr-II and Pr-III phases, one has to metastably pass through the dhcp phase (Pr-I). Obviously, that extrapolation is even more severe for Pr-IV.

The magnitude of the volume collapse in the Pr-III to Pr-IV transition is sensitive to the initial estimation of the EOS fitting parameters. Using the values in Table I, we estimate the volume collapse in this transition as shown in Fig. 5. These graphs do not take into account the presence of the as-yet unidentified Pr-VI phase at temperatures above 670 K, but extrapolates the phase boundary to higher temperatures and pressures. Not surprisingly, given the systematic approach for generating the EOS parameters, the fractional volume change of the transition decreases linearly with temperature: $\Delta V/V(\%) = 16.235 - 0.0156[T(\mathrm{K})]$. Note that the intercept of this line (zero volume collapse) is at 1040 K, which is about 500 K below the melting temperature of Pr at 28 GPa reported by laser heating.[15] The gradual decrease of the volume collapse in Pr appears to be in marked contrast to the rapid decrease of the isostructural volume collapse in Ce as the critical point is approached, the temperature of the critical point being significantly lower than that of the melt. However, the magnitude of the volume collapse decreases as the pressure is increased only because the slope of the Pr-III to Pr-IV boundary (dP/dT) is positive. Since the compressibility of phase III is greater than phase IV, the higher the pressure for the transition the smaller the volume change. This is why determining the structure (and volume) of phase VI is so important. If the transition to phase VI from phase III has no significant volume collapse, and compresses similarly to phase III, then the change in slope (an increase in dP/dT) for the phase VI to IV transition suggests a much more rapidly diminishing volume collapse. Nevertheless, Pr may be analogous in its behavior of the subsequent phase transitions in Ce from γ(fcc) to α'(α-U) then to ε(tetragonal) phases, all of which are electronic in nature.[7,8]

The large volume collapse of Pr is similar to that in Ce in at least one other respect: the change in entropy due to the change in electronic character from localized to itinerant. For the system extrapolated toward $T = 0$ K, the entropy change can be calculated due to the difference in ground-

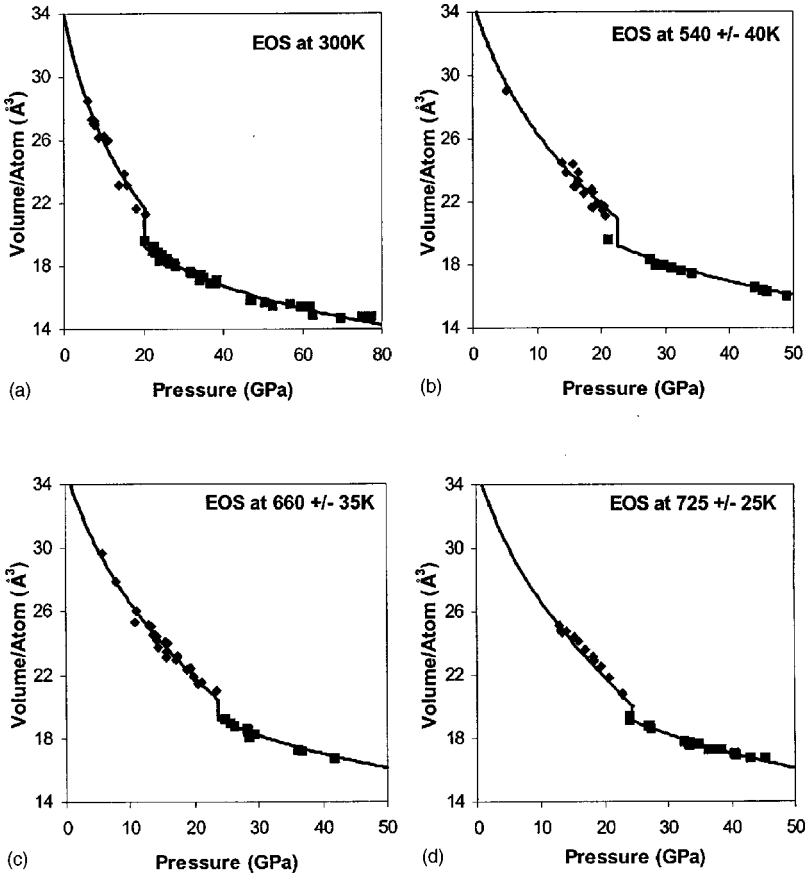

FIG. 4. EOS data for (a) 300 K, (b) 540 K, (c) 660 K, and (d) 725 K. Data have been fitted using values from Table I. Diamonds represent the fcc and distorted-fcc phases. Squares represent the orthorhombic phase.

state multiplicity J. The entropy contribution can be calculated from

$$S = k_B \ln(2J+1). \tag{1}$$

The ground state of the trivalent Pr atom is $^3H_4$, which gives $\Delta S/k_B = 2.197$ since phase IV is itinerant and would effectively have $J=0$. We compare this to the $\Delta S/k_B$ from the Clausius-Clapeyron equation shown below:

$$\Delta S = \Delta V(dP/dT). \tag{2}$$

If we use Fig. 1, we find that the slope of the III-IV boundary is $dP/dT = 9.73$ MPa/K. The 0 K change in volume across that boundary, $\Delta V = 3.29$ Å^3, is calculated from our equation of state data at the extrapolated pressure, also from Fig. 1, of $P = 17.23$ GPa. The result of $\Delta S/k_B = 2.319$ [from Eq. (2)] is in remarkable agreement with the change in entropy calculated from a change in bond character assuming, of course, that the major contribution is from a change in multiplicity. This is analogous to what has been calculated for cerium.[24]

TABLE I. EOS values for Pr-II/Pr-III and for Pr-IV.

fcc+distorted-fcc phases	At 300 K	Δ (per 100 K increase)
B_0 (GPa) (fcc and distorted fcc)	25.1±0.3	0.29±0.051
V_0 (Å^3/atom) (fcc and distorted fcc)	34.2±0.2	0.221±0.022
B' (fcc and distorted fcc)	2.9±0.2	−0.065±0.026
B_0 (GPa) (ortho)	25.7±0.3	0.066±0.020
V_0 (Å^3/atom) (ortho)	27.0±0.3	0.385±0.030
B' (ortho)	4.9±0.1	−0.180±0.020

CONCLUSIONS

The phase diagram of Pr between 5 and 60 GPa from 295 to 830 K has been determined by ADXD and EDXD experiments. There are four phases observed in this region: three previously known phases and a new high-pressure–high-

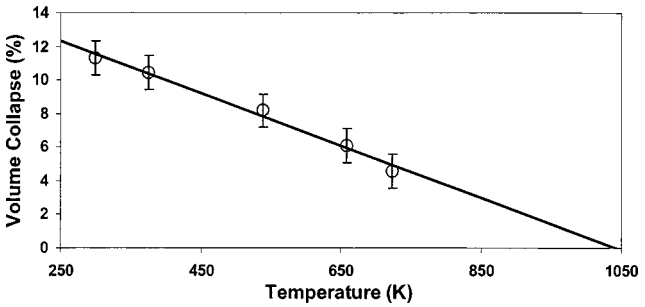

FIG. 5. The volume collapse at the appropriate pressures as a function of temperature. The extrapolation to zero is based on a linear fit following the equation: $\Delta V/V$ (%)=16.235−0.0156 [T(K)].

temperature phase discovered in the present study. We cannot find any evidence for a monoclinic phase. An equation of state for the entire pressure and temperature region of this study has been determined. The selection of mineral oil as a useful hydrostatic pressure medium may be, at best, minimally acceptable at lower temperatures. However, there is clearly a chemical reaction between mineral oil and Pr above 650 K. The fractional volume change of the Pr-III to Pr-IV transition gradually decreases with temperature, extrapolating to zero well below the normal melting temperature. This transition corresponds to a similar volume collapse in cerium where localized *f* electrons become itinerant.

ACKNOWLEDGMENTS

We greatly appreciate K. Visbeck for his experimental assistance and A. McMahan for his invaluable discussions. We also greatly appreciate the efforts and assistance from the staffs at the SSRL and APS, where the present x-ray studies were performed. This work has been supported by the Physics Data Research Program and the Laboratory-Directed Research and Development Program at the Lawrence Livermore National Laboratory, University of California under the auspices of the U.S. Department of Energy under Contract No. W-7405-ENG-48.

[1] A. McMahan, C. Huscroft, R. T. Scalettar, and E. L. Pollock, J. Comput.-Aided Mater. Des. **5**, 131 (1998).
[2] P. Soderlind, Adv. Phys. **47**, 959 (1998).
[3] H. L. Skriver, in *Physics of Solids Under High Pressure*, edited by J. S. Schilling and R. N. Shelton (North-Holland, Amsterdam, 1981).
[4] P. Soderlind, O. Eriksson, B. Johansson, J. M. Wills, and A. M. Boring, Nature (London) **374**, 524 (1995).
[5] J. S. Olsen, L. Gerward, U. Benedict, and J. P. Itie, Physica **133B**, 129 (1985).
[6] Y. K. Vohra and S. L. Beaver, J. Appl. Phys. **85**, 2451 (1999).
[7] D. A. Young, *Phase Diagrams of the Elements* (University of California Press, Berkeley, CA, 1991), Chap. 15, p. 21.
[8] Y. Zhao and W. B. Holzapfel, J. Alloys Compd. **246**, 216 (1997).
[9] J. Akella, G. S. Smith, and A. P. Jephcoat, J. Phys. Chem. Solids **49**, 573 (1988).
[10] R. G. Haire, S. Heathman, and U. Benedict, High Press. Res. **2**, 273 (1990).
[11] M. I. McMahon and R. J. Nelmes, Phys. Rev. Lett. **78**, 3884 (1997).
[12] Y. C. Zhao, F. Porsch, and W. B. Holzapfel, Phys. Rev. B **52**, 134 (1995).
[13] G. N. Chesnut and Y. K. Vohra, Phys. Rev. B **62**, 2965 (2000).
[14] A. Jayaraman, Phys. Rev. **139**, A690 (1965).
[15] D. Errandonea, R. Boehler, and M. Ross, Phys. Rev. Lett. **85**, 3444 (2000).
[16] D. L. Heinz and R. Jeanloz, J. Appl. Phys. **55**, 885 (1984).
[17] N. Hamaya, Y. Sakamoto, H. Fujihisa, Y. Fujii, K. Takemura, T. Kikegawa, and O. Shimomura, J. Phys.: Condens. Matter **5**, L369 (1993).
[18] N. Hamaya, N. Okabe, M. Yamakata, T. Yagi, and O. Shimomura, High Press. Res. **14**, 287 (1996).
[19] W. A. Grosshans, Y. K. Vohra, and W. B. Holzapfel, J. Phys. F: Met. Phys. **13**, L147 (1983).
[20] G. Meyer, ICDB, PDF card 42-0982.
[21] C. Okhi, H. Uchida, and E. Ko, J. Jpn. Inst. Met. **54**, 146 (1990).
[22] F. Birch, J. Appl. Phys. **4**, 279 (1938).
[23] W. J. Carter, J. N. Fritz, S. P. Marsh, and R. G. McQueen, J. Phys. Chem. Solids **36**, 741 (1975).
[24] B. Johansson, I. A. Abrikosov, M. Aldén, A. V. Ruban, and H. L. Skriver, Phys. Rev. Lett. **74**, 2335 (1995).